

## NAVIER-STOKES AND VISCOUS-INVISCID INTERACTION

Joseph L. Steger and William R. Van Dalsem  
NASA Ames Research Center, Moffett Field, California

## INTRODUCTION

A symposium of this type generally attempts to collect two types of papers: papers that present new work and those that try to summarize and act as pathfinders. The latter class of paper is generally written by harried researchers who no longer have time to verify that their ideas seldom work as initially conceived. The reader can readily surmise that this paper belongs to the latter category.

The first part of this paper will simply discuss some considerations toward developing numerical procedures for simulating viscous compressible flows. Both Navier-Stokes and boundary-layer field methods are considered. For the most part, this discussion draws on our own experiences using finite difference procedures and does not pretend to cover the literature. The remaining parts of this paper will deal with two topics with which the authors are involved: 1) a simple formulation for the three-dimensional boundary-layer equations in arbitrary generalized coordinates, and 2) discussion of a technique which we have referred to as the fortified Navier-Stokes (FNS) approach. Both topics are directed towards a long-term effort to build a general purpose compressible flow solver that can optionally take advantage of approximate solution methods both to improve accuracy and efficiency. The three-dimensional boundary-layer procedure in generalized coordinates fulfills a need that we feel has not been adequately satisfied, that is, a simple boundary-layer procedure that can share grids, turbulence models, and even variables with a Navier-Stokes procedure (specifically, a boundary-layer code that does not require special assumptions such as coordinate orthogonality in any one direction). The fortified Navier-Stokes scheme is a procedure that allows approximate techniques or any known information to be incorporated into the Navier-Stokes scheme in a rather benign way. If the approximations break down, the method can still proceed as a less efficient conventional Navier-Stokes solver.

Throughout this paper the question of turbulence modeling will be avoided. Although it is generally acknowledged that current turbulence models are inadequate for complex flow field simulation, our own intuition is that other problems must be dealt with first. Too often, poor results have been blamed on turbulence models when error in specifying boundary conditions and poor grid resolution are the real culprits. Certainly the problem of turbulence modeling cannot be properly assessed until these errors are eliminated and we can routinely deal with complex three-dimensional flows.

## BACKGROUND

Numerical algorithms for viscous flow simulation are designed with several goals in mind. The simulation must be accurate, efficient, and simple and robust so as to minimize the amount of engineering manhours time needed to obtain a solution. Because we do not have sufficient computer resources (and perhaps sufficiently well conditioned algorithms) compromises have to be made. Viscous flow simulation is often carried out using either a coupled boundary-layer inviscid-flow model or the Reynolds-averaged Navier-Stokes equations. For supersonic flow and channel flows, parabolized Navier-Stokes equations which can be marched in attached flow regions have been used as well.

Viscous-inviscid interaction schemes for airfoil analysis have been one and even two orders of magnitude faster than Navier-Stokes schemes, but they have proved to be difficult to generalize to complex three-dimensional separated flow situations and require considerable amount of engineering time to set up. Moreover, the limitations of the boundary-layer equations are not fully understood. For this reason, Navier-Stokes schemes are generally used to simulate complex flows even though they require considerably more computer work per point and usually lead to stiffer sets of equations to solve. Consequently, in viscous flow simulation using the Navier-Stokes equations the computational fluid dynamicist may spend the majority of his or her time trying to make the numerical algorithm more efficient. In viscous flow simulation using matched boundary-layer and inviscid flow equations the main task is to make the codes general enough to reproduce complex flow yet simple enough to economize on the engineering resource. Thus one approach entails making a general scheme more efficient, the other entails making an efficient scheme more general.

### Navier-Stokes

The Navier-Stokes equations are considered to be adequate for most aerodynamic applications and can be used for regions with massive flow separation. Navier-Stokes algorithms that are capable of treating complex geometries use finite difference methods or related finite volume and finite element methods. Because a limited number of grid points are available, regions of massive separation are generally computed in high Reynolds number flow as rotational inviscid flow even though the viscous terms may be retained throughout. Compared to other methods of simulating strongly interacting flows, Navier-Stokes simulation is straightforward and does not require as extensive engineering 'set-up' time as viscous-inviscid interaction methods. However, Navier-Stokes schemes tend to be computer time and storage intensive. As a result, considerable effort is being expended to improve the computational efficiency of Navier-Stokes codes. This effort has, in fact, been successful to the point that algorithm improvements have been keeping pace with improvements in computer hardware. Overall computational efficiency has been improved in a number of ways including use of space varying time steps relaxation variables, use of a sequence of mesh refinements to establish approximate solutions, inclusion of various ways to reduce inversion work, improved numerical dissipation terms, more accurate difference approximations, and more implicit treatment of terms. References 1 to 21 provide one or two pointers to some of the commonly used Navier-Stokes code and descriptions of some the algorithmic changes alluded to above.

Two examples of complex three-dimensional flow simulations carried out with a Navier-Stokes scheme are shown in figures 1 to 4. Figures 1 to 3 show results for jet in a cross flow

which were extracted from reference 22, while figure 4 shows preliminary results ('oil-flow') for supersonic flow over the integrated Space Shuttle vehicle (unpublished work of Buning, Chiu, Obayashi, Rizk, and Steger of a NASA Ames Research Center Space Shuttle flow simulation group). Both results were carried out on one processor of a CRAY 2 computer, used about a quarter of a million grid points, and took from 4 to 8 hours of computer time. Although the jet in cross flow represents a simple configuration, the flow field is complex and more grid resolution (or better numerics) is needed to better resolve the flow features which are unsteady. The simulation of the integrated shuttle vehicle uses a chimera composite grid approach (ref. 23), but binding linkages, plume effects, external fuel feed lines etc. have not yet been modeled.

### Viscous-Inviscid Interaction

Solution algorithms using viscous-inviscid interaction schemes are perhaps equally divided between those which use integral boundary-layer methods and those that use either finite difference or finite element methods — field boundary-layer methods. Integral boundary-layer methods are quite fast and with use of good correlation functions, they can give good accuracy. However, they require modeling of the flow physics, in addition to the turbulence model. As a result it is difficult to decide whether errors are due to turbulence modeling or the integral method modeling. The integral methods also require extensive correlation with experimental data. For these reasons we have preferred field methods over integral methods. (It has also been our experience that once the the boundary-layer and inviscid flow equations are coupled, the computer time savings accrued by using an integral boundary-layer scheme over a field scheme is minimal.)

Compared to Navier-Stokes schemes, viscous-inviscid interaction methods require significantly less computer time to simulate viscous flow with up to small regions of separation. For high Reynolds number flow, accuracy can be equal to Navier-Stokes simulation, however, depending on the problem, engineering 'set-up' time can be higher. For strong viscous interaction, current boundary-layer based schemes tend to break down, although we believe that if the boundary-layer equations can be properly interacted with the inviscid rotational flow equations, for many problems they can give high Reynolds number flow results comparable to the Navier-Stokes equations.

Viscous flow simulation using boundary-layer procedures requires special adaptations and thus has an intensive user workload. For example, if separation is encountered, the boundary-layer algorithm must be converted from the direct to the inverse mode to avoid singular behavior at the separation point. A scheme to update the inverse mode quantity, generally  $\tau_w$  or  $\delta^*$ , must then be provided so that the pressure predicted by the boundary-layer and inviscid schemes are consistent. In conventional viscous - inviscid interaction, the influence of the viscous layer is imposed by displacement thickness or transpiration velocity. An advantage of using either transpiration or an effective body displacement is that the inviscid flow can be computed using a grid that is relatively coarse compared to what is needed for the viscous grid. Moreover, the inviscid grid need not necessarily be body conforming in the way that a high Reynolds number Navier-Stokes grid must be. However, matching to a highly rotational inviscid outer flow is not straightforward; and, in many cases, it is necessary to account for the viscous flow curvature and the pressure gradients of the shear layers.

As an example of the inviscid-viscous interaction approach, the results of computing flow about the RAE 2822 airfoil at  $M_\infty = 0.73$  and  $C_l = 0.803$  are shown. Figures 5 - 7 show

comparisons of the  $C_p$ ,  $C_f$ , and  $\delta^*$  distributions found experimentally (ref. 24), those computed by the interaction method (ref. 25), and those computed by Mehta (ref. 26) using a Navier-Stokes code. Mehta performed his computations at  $\alpha = 2.79^\circ$  (and computed a  $C_l = 0.793$ ); the present computations were performed at  $\alpha = 2.81^\circ$  to match the measured  $C_l = 0.803$ . The present results are in good agreement with both the Navier-Stokes and experimental results. These simulations were obtained on 223x31 inviscid and 223x50 viscous grids using a quite fast transonic full potential code (ref. 27) and equally fast boundary-layer finite difference code (ref. 28). The calculations were carried out in 1984 and for the cases presented, the required Cray-XMP CPU time was 7 to 15 sec, and on the average, 0.0006 sec/grid point were required to obtain a converged solution. In contrast, our most efficient thin-layer Navier-Stokes code at that time (ref. 7) required about 0.03 to 0.06 sec/grid point to obtain a converged solution.

### Zonal Equation Methods

The traditional choice in viscous flow simulation is between either a viscous-inviscid interaction approach using simplified equations or a Navier-Stokes scheme used throughout the field. In practise, however, various kinds of zonal methods are often used. A zonal equation method generally entails regional use of simplified methods with a Navier-Stokes scheme so as to speed up iterative convergence, reduce computational work, or even improve the numerical accuracy of the Navier-Stokes simulations. Simple zonal ideas are almost always used in high Reynolds number flow Navier-Stokes simulations. For example, for high Reynolds number flow, the Navier-Stokes equations revert to Euler equations in any region in which sufficient grid resolution is not provided, so an obvious zonal scheme is to neglect viscous terms in these regions. Special treatment at wall boundaries using 'wall functions' (ref. 29) have also been employed.

In a zonal approach the simplified equations must be able to readily share variables and mesh points with the global scheme. Otherwise, sometimes awkward conversions of variables or messy interpolations between equation sets are required.

One kind of zonal approach is to simply embed Navier-Stokes equations in complex (usually separated or highly vortical) regions of the flow and use simplified equations elsewhere. This requires some care in establishing zones, and the zonal interfacing can be tedious. Alternately a zonal approach can use a global Navier-Stokes and Euler formulation throughout, but use simplified equations embedded into the global scheme to reduce computational work or improve accuracy. The subtle difference between this zonal approach and the former (which is perhaps chiefly observed in the coding) is that, if the approximation behind the simplified equation is no longer valid, simulation can still proceed with the more general scheme. The fortified Navier-Stokes scheme (to be highlighted in a latter Section) and related embedding schemes which use vorticity, potential, and other like forms of the equations (refs. 30-32) are pronounced examples of the latter kind of zonal scheme. An advantage of a general zonal approach is that it is possible to directly compare the effects of using the simplified equation set to the general equation set and thus learn the limitations of the approximation. As experience is gained, it is then likely that the simplified equation sets will be able to assume more of the computational work.

## GENERALIZED BOUNDARY-LAYER EQUATIONS

The boundary-layer equations are restricted to high Reynolds number flow and require the use of a body conforming coordinate system. In developing the usual boundary-layer equations, both the independent variables and the dependent velocity variables are transformed to the new body conforming coordinates. For body surfaces with little curvature, the boundary-layer equations cast in terms of the new dependent variables essentially simplify back to a flat plate or Cartesian-like form of the equations along a developed surface. If the body has appreciable curvature, however, the equations require additional terms and can be difficult to solve numerically. They are particularly more complex if a nonorthogonal coordinate system is used, yet for many applications it is difficult to generate an orthogonal coordinate system along the body surface.

The thin-layer Navier-Stokes equations use body conforming coordinates and only viscous terms in the normal-like direction are retained. With the pressure specified in the viscous layer, the momentum equations of the thin-layer Navier-Stokes equations are readily solved for the original Cartesian velocity components provided only the independent variables are transformed to body coordinates. This is because with pressure specified, the thin-layer momentum equations are essentially equivalent to an uncoupled set of scalar convection-diffusion equations. Moreover, the boundary-layer approximation of specifying the pressure in the viscous layer is equivalent to solving a linear combination of the thin-layer momentum equations – the combination needed to transform the Cartesian velocity components  $u, v$ , and  $w$  into an equivalent normal-like velocity (see ref. 33). Consequently, although three thin-layer momentum equations in transformed independent variables are readily solved for  $u, v$ , and  $w$ , for pressure prescribed in the viscous layer only two linear combinations of the  $u, v$ , and  $w$  velocity components should be retained – the combination that is equivalent to the velocities along the body surface coordinates. Thus equivalent boundary-layer equations can be formulated from the thin-layer equations for pressure specified in the viscous layer; and, because only the independent variables are transformed, complex coordinate source terms can be avoided. Moreover, this alternate form of the boundary-layer equations does not require that any of the coordinates be orthogonal, and software (grids, boundary condition routines, etc.) developed for many Navier-Stokes schemes can be readily utilized.

### Governing Equations

A form of the boundary-layer equations for general curvilinear coordinates  $\xi = \xi(x, y, z)$ ,  $\eta = \eta(x, y, z)$ , and  $\zeta = \zeta(x, y, z)$  is given by reference 33 (with  $\eta$  chosen away from the surface):

$\eta$  Momentum

$$\begin{aligned} \nabla\eta \cdot (\nabla\xi p_\xi + \nabla\eta p_\eta + \nabla\zeta p_\zeta) = & \rho U(u\partial_\xi\bar{\eta}_x + v\partial_\xi\bar{\eta}_y + w\partial_\xi\bar{\eta}_z) \\ & + \rho V(u\partial_\eta\bar{\eta}_x + v\partial_\eta\bar{\eta}_y + w\partial_\eta\bar{\eta}_z) \\ & + \rho W(u\partial_\zeta\bar{\eta}_x + v\partial_\zeta\bar{\eta}_y + w\partial_\zeta\bar{\eta}_z) \end{aligned} \quad (1a)$$

or for very dominant  $\nabla\eta \cdot \nabla\eta$

$$p_\eta = 0 \quad (1b)$$

### $\xi$ and $\zeta$ Momentum

Predict values of  $\vec{q} = (u, v, w)^t$  from

$$\rho u_t + \rho U u_\xi + \rho V u_\eta + \rho W u_\zeta + (\xi_x p_\xi + \eta_x p_\eta + \zeta_x p_\zeta) = J \partial_\eta [J^{-1}(\mu m_1 u_\eta + (\mu/3)m_2 \eta_x)] \quad (2a)$$

$$\rho v_t + \rho U v_\xi + \rho V v_\eta + \rho W v_\zeta + (\xi_y p_\xi + \eta_y p_\eta + \zeta_y p_\zeta) = J \partial_\eta [J^{-1}(\mu m_1 v_\eta + (\mu/3)m_2 \eta_y)] \quad (2b)$$

$$\rho w_t + \rho U w_\xi + \rho V w_\eta + \rho W w_\zeta + (\xi_z p_\xi + \eta_z p_\eta + \zeta_z p_\zeta) = J \partial_\eta [J^{-1}(\mu m_1 w_\eta + (\mu/3)m_2 \eta_z)] \quad (2c)$$

and retain the two linear combinations

$$U = \nabla \xi \cdot \vec{q}$$

$$W = \nabla \zeta \cdot \vec{q}$$

### Energy

$$\rho H_t + \rho u H_\xi + \rho v H_\eta + \rho w H_\zeta - p_t = J \partial_\eta [J^{-1}(\mu m_1 m_3 + (\mu/3)m_2(\eta_x u + \eta_y v + \eta_z w))] \quad (3)$$

where

$$m_1 = \eta_x^2 + \eta_y^2 + \eta_z^2$$

$$m_2 = \eta_x u_\eta + \eta_y v_\eta + \eta_z w_\eta$$

$$m_3 = [(u^2 + v^2 + w^2)_\eta]/2 + Pr^{-1}(\gamma - 1)^{-1}(a^2)_\eta$$

### Constitutive

$$\frac{\rho}{\rho_\infty} = \frac{p T_\infty}{p_\infty T} \quad (4a)$$

where

$$\frac{T}{T_\infty} = \frac{(\gamma - 1)}{a_\infty^2} \left[ H - \frac{(u^2 + v^2 + w^2)}{2} \right] \quad (4b)$$

### Continuity

$$(J^{-1} \rho)_\tau + (J^{-1} \rho U)_\xi + (J^{-1} \rho V)_\eta + (J^{-1} \rho W)_\zeta = 0 \quad (5)$$

Throughout  $\rho$ ,  $p$ , and  $T$  denote fluid density, pressure, and temperature,  $u, v, w$  are Cartesian velocity components referenced to an inertia system,  $H$  is the stagnation enthalpy,  $a$  is the sound speed, and  $\mu$  is the viscosity coefficient. The transform Jacobian is given by  $J = \left| \frac{\partial(\xi, \eta, \zeta)}{\partial(x, y, z)} \right|$ , and

the overbar on  $\eta_x$ ,  $\eta_y$ , and  $\eta_z$  denotes scaling,  $\bar{\eta}_x = \eta_x / \sqrt{\eta_x^2 + \eta_y^2 + \eta_z^2}$  etc. The operator  $\vec{\nabla}$  denotes the vector gradient so that  $\vec{\nabla}\eta \cdot \vec{q} = \eta_x u + \eta_y v + \eta_z w = V$ , and  $V$  is the vertical contravariant velocity.

The six equations ( $\eta$  momentum (1); two linear combinations of (2a), (2b), and (2c) to form  $U$  and  $W$ ; energy (3); state (4a); and continuity (5)) can be used to determine the six variables  $p, U, W, H, \rho, V$ . The Cartesian velocity components are then obtained from

$$\begin{pmatrix} u \\ v \\ w \end{pmatrix} = \begin{bmatrix} x_\xi & x_\eta & x_\zeta \\ y_\xi & y_\eta & y_\zeta \\ z_\xi & z_\eta & z_\zeta \end{bmatrix} \begin{pmatrix} U \\ V \\ W \end{pmatrix} \quad (6)$$

### Numerical Scheme

This formulation has been applied to steady state problems using the time-like boundary-layer scheme reported by Van Dalsem and Steger in reference 34. For a prescribed edge pressure, the equations are solved iteratively from an assumed initial state in the following way with  $p_\eta = 0$ . Using central spatial differencing in  $\eta$  and upwind differencing in  $\xi$  and  $\zeta$ , equations (2) to (3) are used to update  $u, v, w$ , and  $H$ . As pressure was already obtained using one linear combination of the momentum equations, only two linear combinations of the momentum equations can be used to determine the velocities. Thus,  $U$  and  $W$  are formed from  $u, v$ , and  $w$ . The equation of state, (4a), is used to update  $\rho$ , with  $T$  defined from equation (4b). The third linear combination of  $u, v, w$  is obtained by solving continuity for  $V$  using already updated  $U, W$ , and  $\rho$ . The continuity equation has central space differencing in  $\xi$  and  $\zeta$ , and trapezoidal differencing in  $\eta$  so that  $V$  is obtained by marching outwards from the body surface. The final updated form of the Cartesian velocity components is then obtained from updated  $U, V, W$  using equation (6). This process is then repeated until convergence.

The boundary-layer equations are solved with either specified initial data profiles or the stagnation region can be captured with the upwind differencing as part of the iteration process. At the outer edge in  $\eta$ , variables can be specified if known, or, for specified edge pressure, the edge variables can be computed as part of the boundary-layer method. In this case the  $\rho V \partial_\eta$  terms in momentum and energy are backward differenced away from the edge if  $V > 0$ , or dropped if  $V < 0$ . Likewise the viscous terms must be dropped at just the outer edge point. Periodic, symmetry, or outflow conditions are used at all other  $\xi$  and  $\zeta$  boundaries at which initial data are not specified.

### Numerical Results

Boundary-layer calculations to verify this formulation have been carried out on a 6 : 1 prolate spheroid at 10° and 30° angle of attack and at two different Reynolds numbers,  $7.7 \times 10^6$  and  $43 \times 10^6$  based on diameter. The geometry and a top view of the computed limiting streamlines for the 30° angle of attack case are shown in figure 8. Streamwise separation was avoided by confining the boundary-layer calculation from  $x/L = 0.02$  to  $x/L = 0.8$  where  $x$  is the axial distance and  $L$  is the body length. The initial profiles in  $\xi$ , edge conditions, turbulent eddy viscosity values, and even the grid itself were taken from the Navier-Stokes calculations described in reference 35. Throughout, the simplified  $\eta$  momentum equation,  $p_\eta = 0$ , was used.

As reported in references 33 and 35, good agreement between the boundary-layer method, the Navier-Stokes calculation and even experiment is obtained for attached flow regions. For latter reference, a boundary-layer computed profile at  $x/L = 0.65$  and  $\phi = 120^\circ$  ( $\phi = 0^\circ$  is the windward plane of symmetry) is shown in figure 9 along with the computed thin-layer Navier-Stokes result.

Calculations were also carried out for the  $10^\circ$  case in which the boundary-layer code was run from  $x/L = 0.8$  to  $x/L = 1.1$  - the latter  $x/L$  location is back on the supporting sting which was modeled in the Navier-Stokes simulation. In this region streamwise separation occurs. As shown by the separated profile at  $x/L = 0.96$  and  $\phi = 120^\circ$ , figure 10, the boundary-layer equations solved in the direct mode break down very rapidly unless the outer 'edge' is taken very close to the wall. To prevent breakdown the constant height edge had to be taken so sufficiently close that for this profile the flow is not just rotational but still fully viscous. Breakdown of the boundary-layer equations in direct mode (i.e. pressure specified) is not surprising. Of interest, though, is that the boundary-layer equations do give good results in the direct mode provided that good outer edge values (not irrotational values) are given sufficiently close to the wall.

## FORTIFIED NAVIER-STOKES

In a typical high-Reynolds number Navier-Stokes simulation the fine-grid resolution is generally provided in a thin zone near the body surface, and the outer flow is effectively resolved as rotational inviscid flow (unless the turbulent coefficients are quite large, in which case extensive modeling is required). Because of the fine-grid resolution required near the body, a given algorithm often operates much less efficiently on the Navier-Stokes equations than it does on the Euler equations, even though the work per step may be similar and the viscous terms may enhance stability. However, on this same refined viscous grid, the boundary-layer equations can be efficiently and accurately solved. As a result one can speculate that by using a boundary-layer algorithm near the wall, it may be possible to significantly improve the productivity of the Navier-Stokes algorithm. A convenient way of imposing the boundary-layer equations in this way is by a general method which we have termed fortified Navier-Stokes (FNS).

### Fortified Approach

As an alternative to the traditional "zonal" concept of solving the various flow zones on separate grids and patching the zones together, the Navier-Stokes equations can be applied throughout and the solution of simplified or subset equations can be embedded into the more general or global algorithm by means of a forcing function (fig. 11). In this way, the approximate solution scheme is used to enhance or "fortify" the more general scheme so as to improve the overall accuracy or efficiency. For example, the thin-layer Navier-Stokes equations can be represented in a form

$$\partial_\tau(\hat{Q}) + \partial_\zeta(\hat{F}) + \partial_\eta(\hat{G}) + \partial_\zeta(\hat{H}) = Re^{-1} \partial_\eta \hat{S}$$

where  $\hat{Q}$  is the solution vector,  $\hat{F}$ ,  $\hat{G}$ , and  $\hat{H}$  are flux terms, and  $\hat{S}$  is the viscous stress term in  $\eta$ . These equations can be fortified through the addition of a dissipative forcing term as (refs. 36-38)

$$\partial_\tau(\hat{Q}) + \partial_\xi(\hat{F}) + \partial_\eta(\hat{G}) + \partial_\zeta(\hat{H}) = Re^{-1}\partial_\eta\hat{S} + \bar{C}(\hat{Q}_{bl} - \hat{Q}) \quad (7)$$

where  $\hat{Q}_{bl}$  denotes  $\hat{Q}$  formed from the boundary-layer solution. The positive definite operator  $\bar{C}$  is chosen such that  $-\bar{C}\hat{Q}$  is a damping term and is easily invertable, for example

$$\bar{C} = \chi I \quad (8a)$$

with  $I$  the identity, or

$$\bar{C} = -\chi(\partial_{\xi\xi} + \partial_{\eta\eta} + \partial_{\zeta\zeta}) \quad (8b)$$

The parameter  $\chi$  is picked as a large positive coefficient that blends to zero outside of the forced region of the viscous layer. Inside the viscous layer  $\hat{Q}_{bl}$  approaches  $\hat{Q}$  so no error is generated by the addition of the term  $\bar{C}(\hat{Q}_{bl} - \hat{Q})$ . For a frozen  $\hat{Q}_{bl}$ , such an implicitly imposed forcing term can be used to favorably alter the stability properties of numerical solution algorithms. (Analysis of this approach has been presented in references 37 and 38.) Outside of the forced region of the viscous layer  $\chi$  is zero and only the thin-layer Navier-Stokes equations are solved.

By adding subset equation forcing terms to the Navier-Stokes equations, the Navier-Stokes and subset equations interact strongly over entire regions rather than just at interface boundaries. Moreover, the subset equations can be applied selectively to only those regions where they are clearly valid. In principle, if during an iterative solution process the approximation method become suspect in a certain region, the forcing can be turned off, and the region can be resolved with only the global Navier-Stokes scheme. Because of this flexibility, the generality of the Navier-Stokes equations is retained with the FNS approach, while some of the efficiency of the subset algorithms is recovered.

### Numerical Implementation

The fortified terms have been implemented in an implicit approximately factored algorithm for the three-dimensional thin-layer Navier-Stokes equations written in general coordinates. The basic two-factor solution algorithm (refs. 14, 15) uses central spatial differencing in the  $\eta$  and  $\zeta$  directions and upwinding in the  $\xi$  direction. The forcing term with  $\bar{C} = \chi I$  has been added to the basic algorithm as (refs. 37,38)

$$\begin{aligned} & \left[ I(1 + h\chi) + h\delta_\xi^b(\hat{A}^+)^n + h\delta_\zeta\hat{C}^n - hRe^{-1}\bar{\delta}_\zeta J^{-1}\hat{M}^n J - D_i|_\zeta \right] \\ & \times [I(1 + h\chi)]^{-1} \times \left[ I(1 + h\chi) + h\delta_\xi^f(\hat{A}^-)^n + h\delta_\eta\hat{B}^n - D_i|_\eta \right] \Delta\hat{Q}^n = \\ & - \Delta t \{ \delta_\xi^b[(\hat{F}^+)^n - \hat{F}_\infty^+] + \delta_\xi^f[(\hat{F}^-)^n - \hat{F}_\infty^-] + \delta_\eta(\hat{G}^n - \hat{G}_\infty) + \delta_\zeta(\hat{H}^n - \hat{H}_\infty) \\ & - Re^{-1}\bar{\delta}_\zeta(\hat{S}^n - \hat{S}_\infty) \} - (D_e|_\eta + D_e|_\zeta)(\hat{Q}^n - \hat{Q}_\infty) + h\chi(\hat{Q}_f - \hat{Q}^n) \end{aligned} \quad (9)$$

Here  $h = \Delta t$  (first order in time), or  $h = \frac{\Delta t}{2}$ , (second order in time) and a free stream base solution is subtracted out to improved accuracy in the far field. The operators  $\delta_\xi^b$  and  $\delta_\xi^f$  are backward and forward three-point difference operators. The flux  $\hat{F}$  has been eigensplit and the matrices  $\hat{A}$ ,  $\hat{B}$ ,  $\hat{C}$ , and  $\hat{M}$  result from local linearization of the fluxes about the previous time level. Because central-space-difference operators are used in  $\eta$  and  $\zeta$ , implicit  $D_i$  and explicit

$D_e$  numerical dissipation terms are included in equation (9). With this implementation,  $\chi$  can become very large without concern for large factorization errors, and  $\chi$  contributes to the diagonal dominance of both left-hand factors.

## Results

The FNS method has been tested on a simple geometry which roughly models an infinitely swept wing - a 7.75% thick sine-wave bump-on-a-wall with a 35° leading edge sweep. The flow was computed with a thin-layer Navier-Stokes algorithm (refs. 14,15) and with the FNS scheme using the Van Dalsem and Steger boundary-layer field method (ref. 34). The flow was first computed using the standard Navier-Stokes algorithm alone on both a fine mesh (29 points in the flow direction, 50 points normal to the wall, 5 points in the span direction) and a coarse mesh which has only 20 points in the critical normal direction. The same minimum normal spacing at the wall was used in both the coarse- and fine-mesh computations. This flow was also computed with the FNS approach using the coarse Navier-Stokes mesh (20 points in the normal direction) and, near the wall, a superimposed fine boundary-layer mesh (50 points in the normal direction). In all the FNS computations presented here,  $\chi$  was proportional to the vorticity; hence, it is automatically large within the boundary-layer and rapidly drops to zero near the edge of the boundary-layer. The drag history in figure 12 shows that the coarse-grid standard Navier-Stokes computation does not predict the drag accurately, and that the FNS method obtains essentially the same drag level in 50 iterations that the fine-grid standard Navier-Stokes computation reached in 400 iterations. The computed near-surface particle traces are shown in figures 13a-c. Both the FNS method and the fine-grid standard Navier-Stokes computations predict a constant chord-line separation line, whereas the coarse-grid standard Navier-Stokes computation does not quite capture this qualitative feature.

The swept infinite wing geometry described above was modified to yield a three-dimensional flow by reducing the aspect ratio of the wing to one. Also, to resolve spanwise changes, the grid dimension in this direction was increased from 5 to 15. The resulting particle traces (figs. 14a-d) show the same trends as described for the infinite span example. Also shown in figure 14d is the result obtained when the viscous terms and no-slip boundary conditions are removed from the global numerical algorithm (thus making it an Euler formulation). In this case, the entire influence of viscosity must be carried by the boundary-layer algorithm, which is not a difficulty for this case. The drag history versus CRAY-XMP CPU time for these computations is presented in figure 15. As before, the coarse-grid standard Navier-Stokes computation is not accurate, and the fine-grid standard Navier-Stokes computation is expensive, whereas the FNS (and Euler) computations yield the same drag level as does the fine-grid standard Navier-Stokes computation, but for one-twentieth of the cost.

## CONCLUDING REMARKS

Because efficient viscous-inviscid interaction methods have been difficult to extend to complex three-dimensional flow simulations, Navier-Stokes procedures are more frequently being utilized even though they require considerably more work per grid point. It would seem a mistake, however, not to make use of the more efficient approximate methods in those regions in which they are clearly valid. Ideally we should like a general purpose compressible flow solver that can optionally take advantage of approximate solution methods both to improve accuracy and efficiency. Some potentially useful steps toward this goal have been described in this paper — a generalized three-dimensional boundary-layer formulation and the fortified Navier-Stokes procedure. Further work remains in merging these steps and more.

## REFERENCES

1. MacCormack, R. W.: Current Status of Numerical Solutions of the Navier-Stokes Equations. AIAA Paper No. 85-0032, Jan., 1985.
2. Shang, J. S.: An Assessment of Numerical Solutions of the Compressible Navier-Stokes Equations. AIAA J. of Aircraft, Vol. 2, No. 5, May 1985, pp 353-370.
3. Holst, T.L.: Numerical Solution of the Navier-Stokes Equations About Three-Dimensional Configurations — A Survey. Presented at the NASA Conference on Supercomputing in Aerospace, Moffett Field, CA, March 10-12, 1987.
4. Briley, W. R. and McDonald, H.: Solution of the Multidimensional Compressible Navier-Stokes Equations by a Generalized Implicit Method. J. Comp Physics, Vol. 24, No. 4, August, 1977.
5. Warming, R. F. and Beam, R. M.: On the Construction and Application of Implicit Factored Schemes for Conservation Laws. Symposium on Computational Fluid Dynamics, New York, April 1977, SIAM-AMS Proceedings, Vol. 11, 1977.
6. Pulliam, T. H. and Steger, J. L.: On Implicit Finite Difference Simulations of Three-Dimensional Flows. AIAA J., Vol. 18, Feb. 1979.
7. Pulliam, T. H. and Steger, J. L.: Recent Improvements in Efficiency, Accuracy, and Convergence of an Implicit Approximate Factorization Algorithm. AIAA Paper 85-0360 Jan. 1985
8. MacCormack, R. W.: A Numerical Method for Solving the Equations of Compressible Viscous Flow. AIAA 81-0110, Jan. 1981.
9. Shang, J. S. and Scherr, S. J.: Navier-Stokes Solution of the Flow Field Around a Complete Aircraft. AIAA Paper No. 85-1509, July, 1985.
10. Thomas, J. L. and Walters, R. W.: Upwind Relaxation Algorithms for the Navier-Stokes Equations. AIAA Paper No. 85-1501 CP, July 1985.
11. Thomas, J. L., Taylor, S. L. and Anderson, W. K.: Navier-Stokes Computations of Vortical Flows Over Low Aspect Ratio Wings. AIAA-87-0207, Reno, Nevada, January 1987.
12. Holst, T. L., Kaynak, U., Gundy, K. L., Thomas, S. D., Flores, J., and Chaderjian, N.: Numerical Solution of Transonic Wing Flows Using an Euler/Navier-Stokes Zonal Approach. AIAA Paper No. 85-1640, July, 1985.
13. Flores, J., Holst, T. L., Kaynak, U., Gundy, K. and Thomas, S. D.: Transonic Navier-Stokes Wing Solution Using a Zonal Approach. Part 1. Solution Methodology and Code

Validation. AGARD 58th Fluid Dynamics Panel Symposium, Aix-en-Provence, France, April, 1986.

14. Ying, S. X., Steger, J. L., Schiff, L. B., and Baganoff, D.: Numerical Simulation of Unsteady, Viscous, High Angle of Attack Flows Using a Partially Flux-Split Algorithm. AIAA Paper No. 86-2179, Aug. 1986.

15. Steger, J. L., Ying, S. X., and Schiff, L.B.: A Partially Flux-Split Algorithm for Numerical Simulation of Compressible Inviscid and Viscous Flow. *Proceedings of the Workshop on Computational Fluid Dynamics*, Institute of Nonlinear Sciences, University of California, Davis, California, 1986.

16. Rai, M. M.: Navier-Stokes Simulations of Rotor-Stator Interaction Using Patched and Overlaid Grids. AIAA Paper No. 85-1519, July, 1985.

17. Chima, R. V.: Development of an Explicit Multi-Grid Algorithm for Quasi-Three-Dimensional Viscous Flows in Turbo Machinery. NASA TM 87128, Jan. 1986.

18. Kumar, A.: Numerical Simulation of Scramjet Inlet Flow Fields. NASA TP-2517, May 1986.

19. Chakravarthy, S. R.: Relaxation Methods for Unfactored Schemes. AIAA Paper 84-0165, Jan. 1984.

20. Shankar, V. and Chakravarthy, S.: Development and Application of Unified Algorithms for Problems in Computational Science. NASA Conference Publication 2454, Supercomputing in Aerospace, March 1987.

21. Fujii, K. and Schiff, L. B.: Numerical Simulation Over a Strake-Delta Wing. AIAA-87-1229, Honolulu, Hawaii, June 1987.

22. Van Dalsem, W. R., Panaras, A. G., and Steger, J. L.: Numerical Investigation of a Jet in Ground Effect with a Crossflow. Proceedings of the 1987 SAE International Powered Lift Conference and Exposition, Santa Clara, CA, Dec. 7-10, 1987.

23. Benek, J. A., Buning, P.G., and Steger, J.L.: A 3-D Chimera Grid Embedding Technique. AIAA Paper No. 1523, AIAA 7th Computational Fluid Dynamics Conference. Cincinnati, Ohio, July 15-17, 1985.

24. Cook, P. H., McDonald, M. A., and Firmin, M. C. P.: Aerofoil RAE 2822-Pressure Distributions and Boundary-Layer and Wake Measurements. AGARD AR 138, Paper A6, 1979.

25. Van Dalsem, W. R., and Steger, J. L.: Finite-Difference Simulation of Transonic Separated Flow Using a Full Potential-Boundary Layer Interaction Approach. AIAA Paper 83-1689, Presented at the 16th Fluid and Plasma Dynamics Conference, Danvers, Massachusetts, July 12-14, 1983.

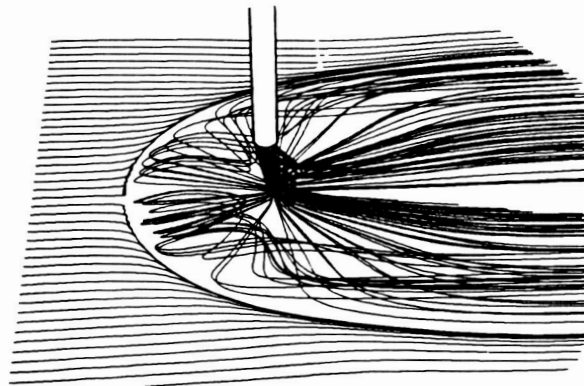
26. Mehta, U.: Reynolds Averaged Navier-Stokes Computations of Transonic Flows Around Airfoils. Presented at the Second Symposium on Aerodynamic Flows, Long Beach, California, January 17-20, 1983.

27. Dougherty, F. C., Holst, T. L., Gundy, K. L., and Thomas, S. D.: TAIR - A Transonic Airfoil Analysis Computer Code. NASA TM-81296, 1981.

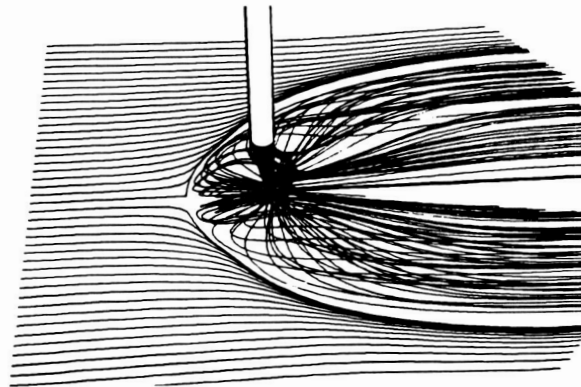
28. Van Dalsem, W. R.: Simulation of Separated Transonic Airfoil Flow by Finite-Difference Viscous-Inviscid Interaction. Ph.D. Thesis, Stanford University, June 1984.

29. Rubesin, M. W. and Viegas, J. R.: A Critical Examination of the Use of Wall Functions as Boundary Conditions in Aerodynamic Calculations. Third Symposium on Numerical and Physical Aspects of Aerodynamic Flows, California State University, Long Beach, Calif., Jan. 1985.

30. Hafez, M. M., Habashi, W. G., Przybytkowski, S. M. and Peeters, M. F.: Compressible Viscous Internal Flow Calculations by a Finite Element Method. AIAA Paper No. 87-0644, Jan. 1987.
31. Davis, R. L., Carter, J. E., and Hafez, M. M.: Three-Dimensional Viscous Flow Solutions with a Vorticity-Stream Function Formulation. AIAA Paper No. 87-0601, Jan. 1987.
32. Rao, K. V., Pletcher, R. H., Steger, J. L., and Van Dalsem, W. R.: A Three-Dimensional Dual-Potential Procedure with Applications to Wind Tunnel Inlets and Interacting Boundary-Layers. Iowa State University, Report ISU-ERI-87296, June 1987.
33. Steger, J. L. , Van Dalsem, W. R., Panaras, A. G., and Rao, K. V., A Formulation for the Boundary-Layer Equations in General Coordinates. NASA TM 100079, 1988.
34. Van Dalsem, W. R. and Steger, J. L. Efficient Simulation of Separated Three-Dimensional Viscous Flows Using the Boundary-Layer Equations, AIAA J. Vol. 25, no. 3, pp. 395-400, 1987.
35. Panaras, A. G. and Steger, J. L. : A Thin-Layer Navier-Stokes Solution of the Flow about a Prolate Spheroid, AGARDOGRAPH, Report of WG 10, Yoshihara, H. ed., 1988.
36. Steger, J. L., and Van Dalsem, W. R.: Developments in the Simulation of Separated Flows Using Finite-Difference Methods. *Proceedings of the Third Symposium on Numerical and Physical Aspects of Aerodynamic Flows*, California State University, Long Beach, California, 1985.
37. Van Dalsem, W. R., and Steger, J. L.: Using the Boundary-Layer Equations in Three-Dimensional Viscous Flow Simulation. *Proceedings of the 58th Meeting of the AGARD Fluid Dynamics Panel Symposium on Applications of Computational Fluid Dynamics in Aeronautics*, Aix-en-Provence, France, 1986.
38. Van Dalsem, W. R. and Steger, J. L.: The Fortified Navier-Stokes Approach. Proceedings of the Workshop on Computational Fluid Dynamics held by the Institute of Nonlinear Sciences at the University of California, Davis, June 17-18, 1986.



a. (laminar)



b. (turbulent)

Figure 1. Jet in ground effect issuing into a crossflow with  $\frac{V_\infty}{V_{jet}} = 0.223$  and a nozzle height located 3 jet diameters above the wall.

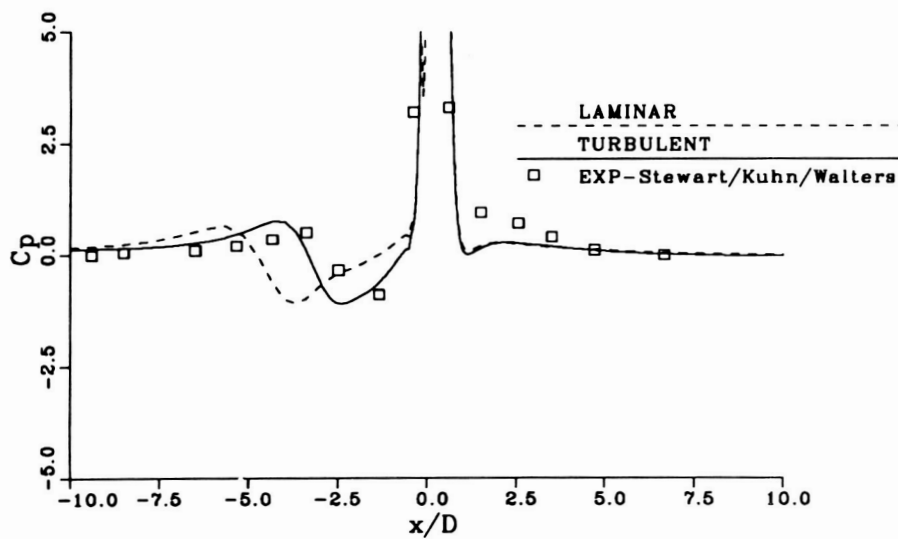


Figure 2. Centerline  $C_p$  distributions for the jet in ground effect with  $\frac{V_\infty}{V_{jet}} = 0.223$  and a nozzle height located 3 jet diameters above the wall.

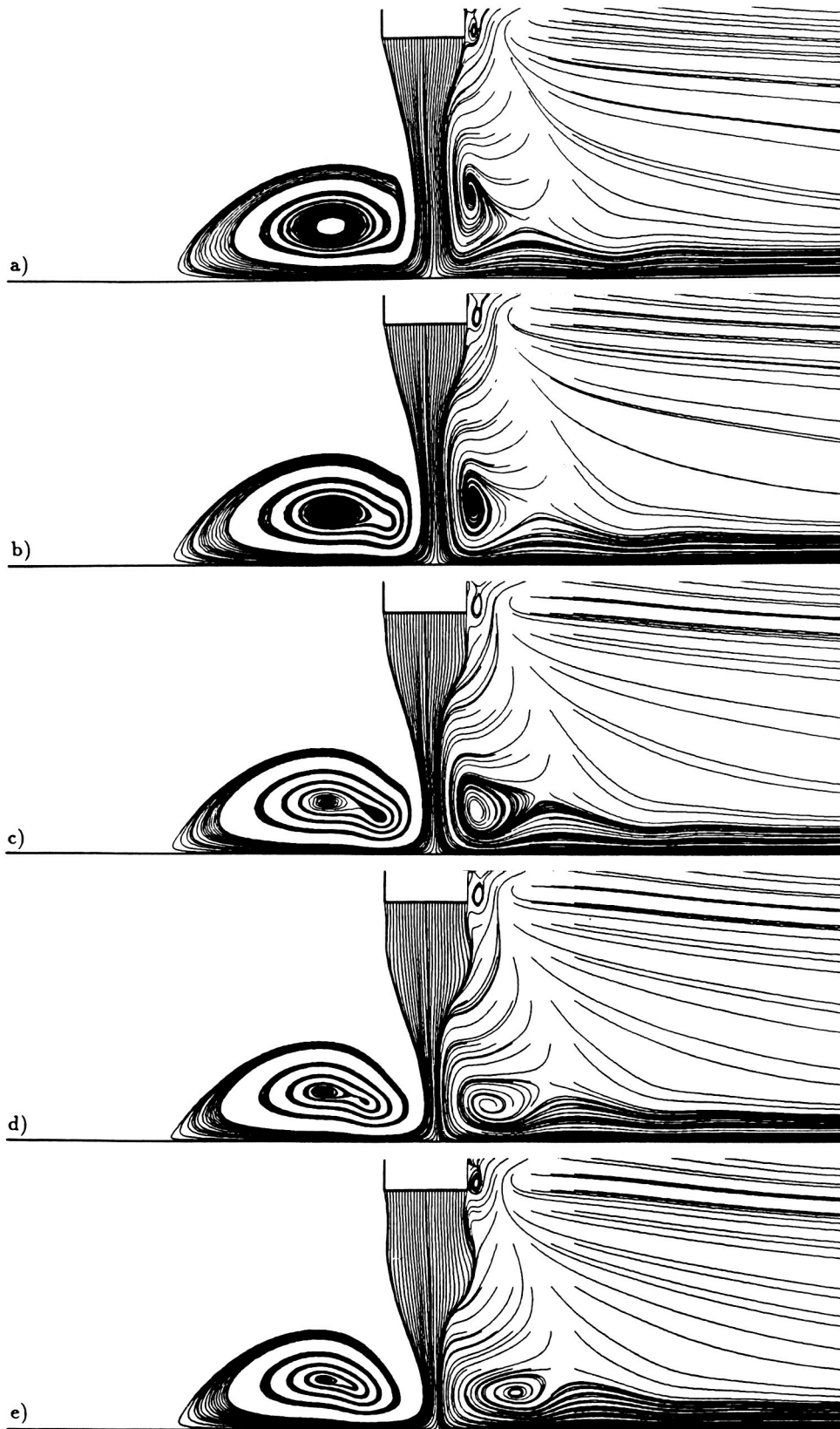


Figure 3. Time history of particle traces indicating the interaction of the ground vortex and the ring vortex.

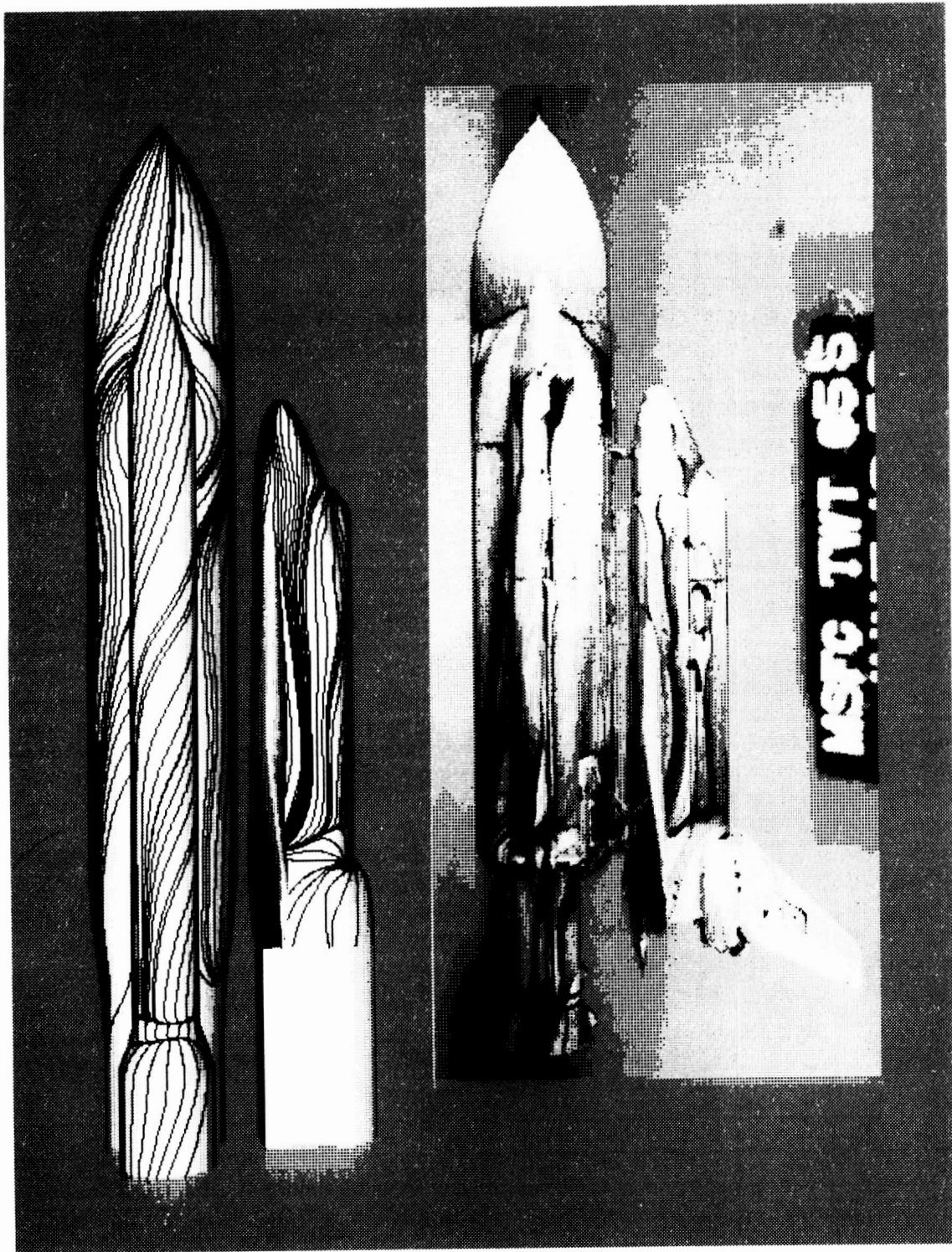


Figure 4. Simulated oil flow (limiting streamlines) compared to experiment for the integrated space shuttle at  $M_\infty = 2.0, \alpha = -4^\circ$ .

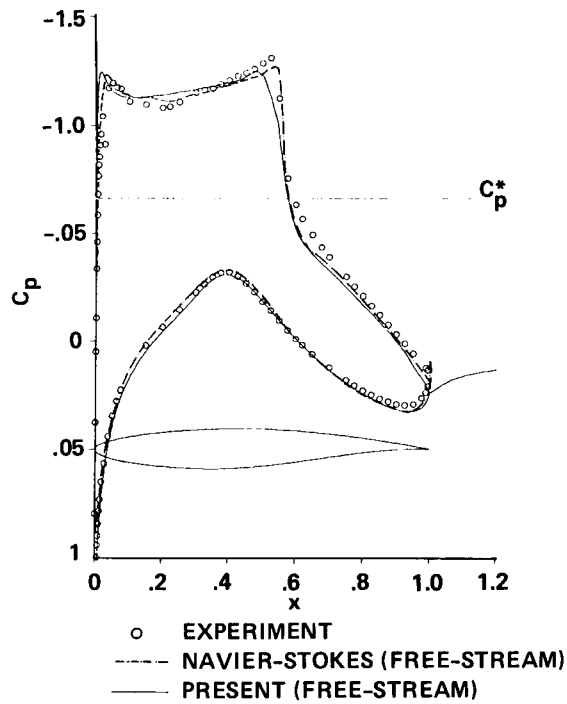


Figure 5. Computed and experimental pressure distributions for RAE 2822 airfoil at  $M_\infty = 0.73$ ,  $Re_\infty = 6.50 \times 10^6$ ,  $C_l = 0.803$ .

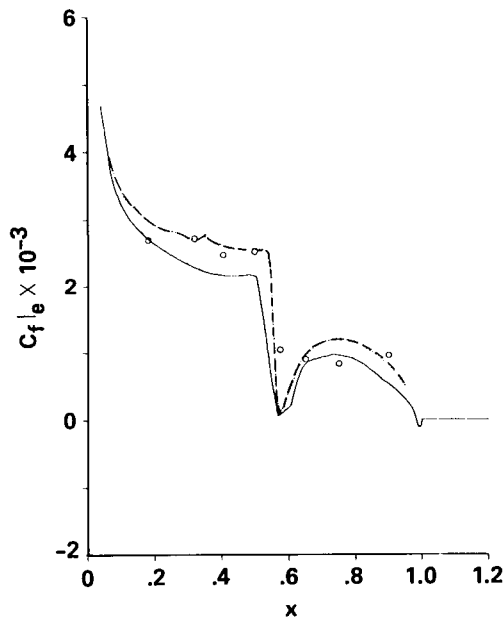


Figure 6. Computed and experimental  $C_{f|e}$  distributions for RAE 2822 airfoil at  $M_\infty = 0.73$ ,  $Re_\infty = 6.50 \times 10^6$ ,  $C_l = 0.803$ .

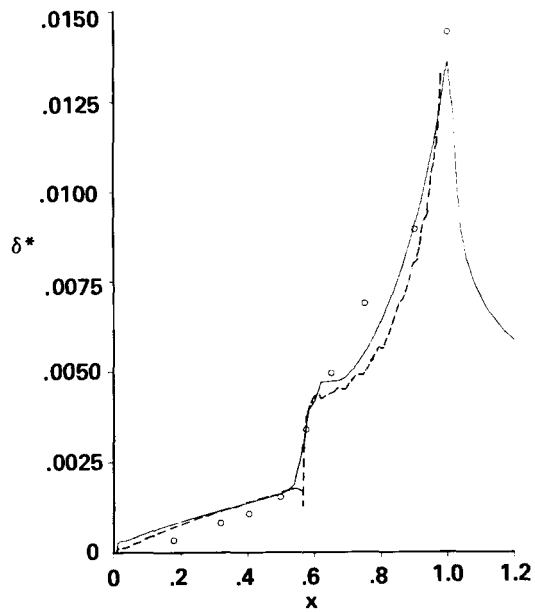


Figure 7. Computed and experimental  $\delta^*$  distributions for RAE 2822 airfoil at  $M_\infty = 0.73$ ,  $Re_\infty = 6.50 \times 10^6$ ,  $C_l = 0.803$ .

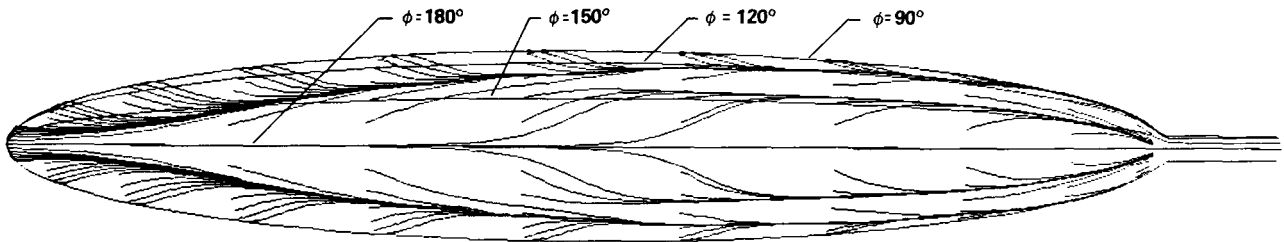


Figure 8. Top view of 6 : 1 prolate spheroid showing thin-layer Navier-Stokes and boundary-layer ( $0.02 \leq x/L \leq 0.80$ ) computed limiting streamlines for  $M_\infty = 0.25$ ,  $\alpha = 30^\circ$ , and  $Re = 43 \times 10^6$ .

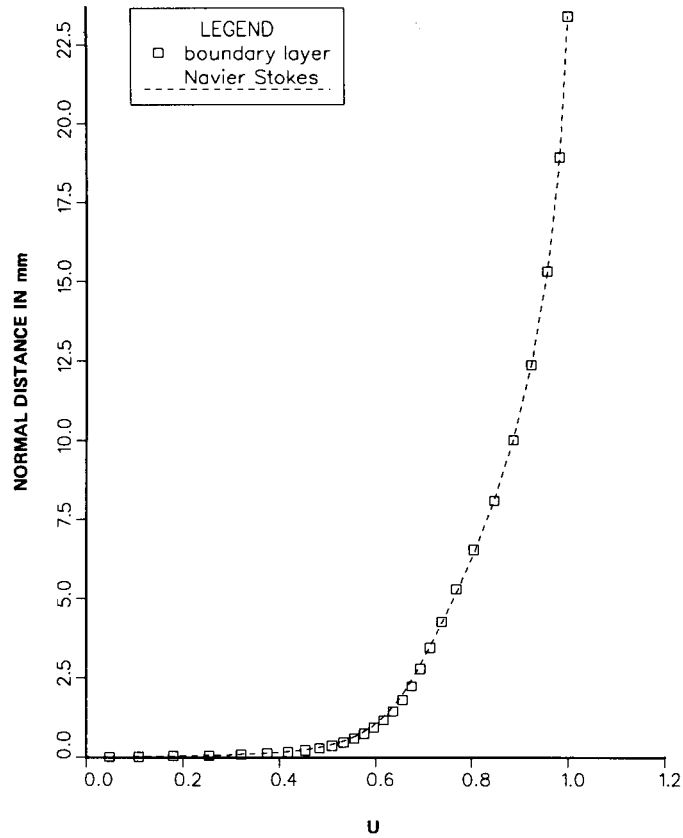
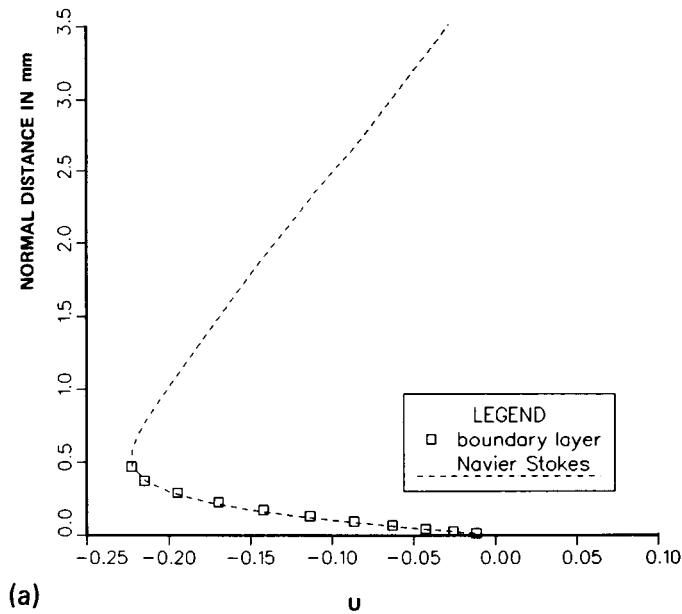


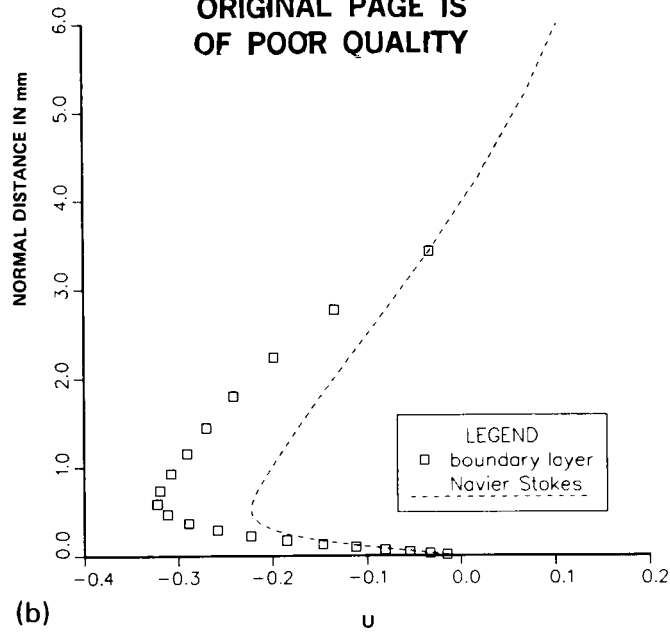
Figure 9. A typical computed attached profile (contravariant  $U$  versus normal height) at  $x/L = 0.65$  and  $\phi = 120^\circ$  on the prolate spheroid at  $10^\circ$  angle of attack using boundary-layer and thin-layer Navier-Stokes equations.



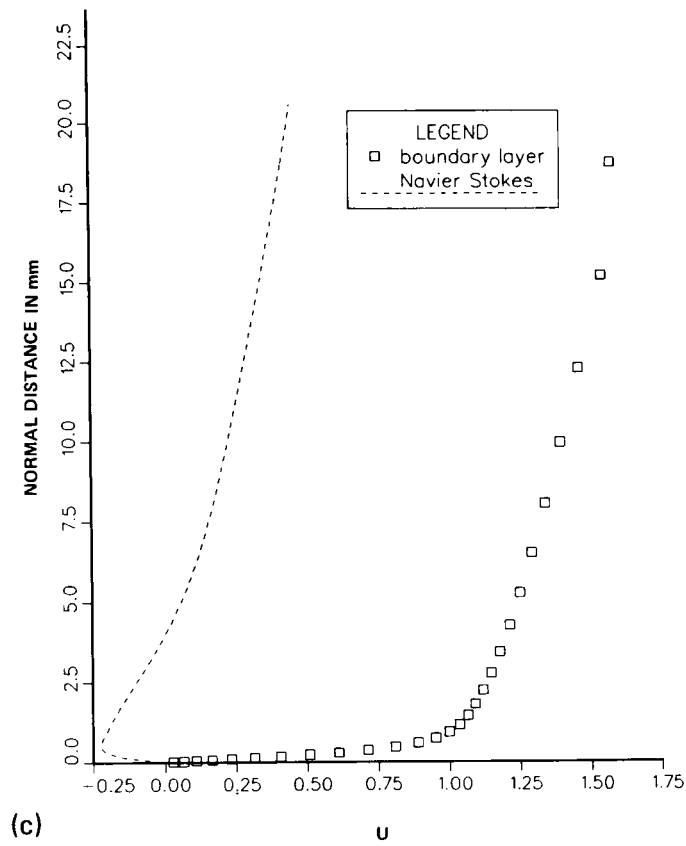
(a)

Figure 10. A separated profile at  $x/L = 0.96$  and  $\phi = 120^\circ$  on the prolate spheroid at  $10^\circ$  angle of attack showing breakdown of the direct mode boundary-layer computation as the outer edge is moved away from the wall.

ORIGINAL PAGE IS  
OF POOR QUALITY



(b)



(c)

Figure 10. Concluded.

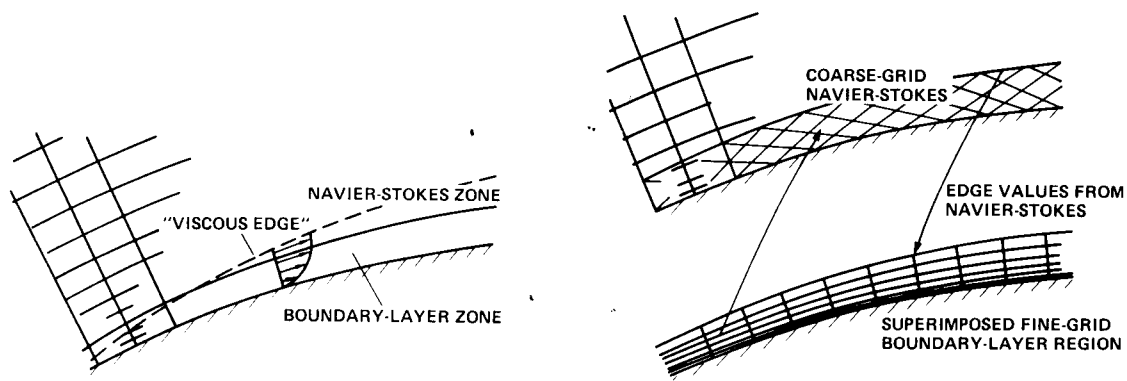


Figure 11. Boundary-layer forced Navier-Stokes schemes.

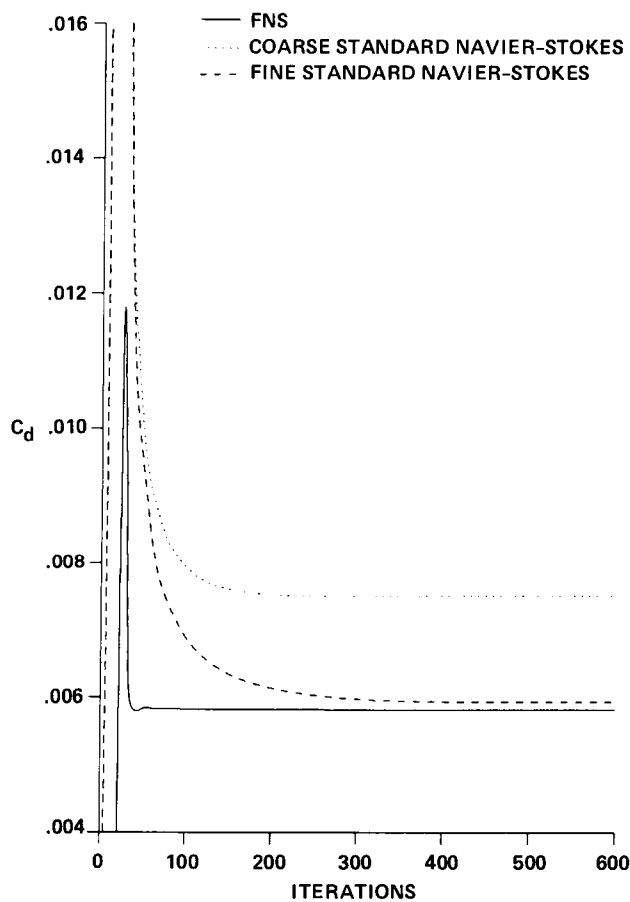


Figure 12. Drag coefficient history versus iterations for the turbulent flow over a 7.75% sine wave bump with a 35° leading-edge sweep,  $Re = 5 \times 10^5$ , and  $M_\infty = 0.5$ .

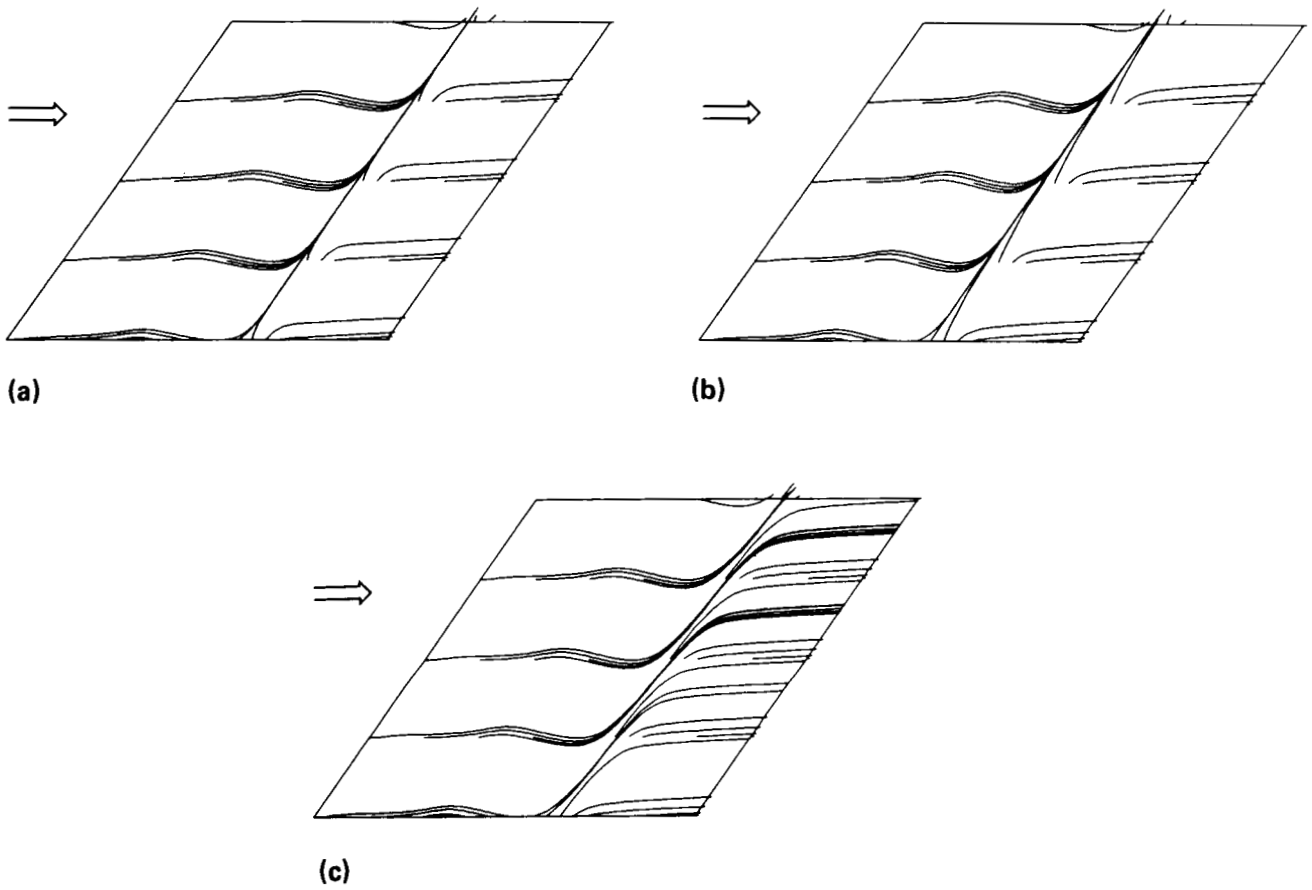


Figure 13. Computed near-surface particle traces for the bump flow: a) Fortified Navier-Stokes; b) standard Navier-Stokes (fine mesh); c) standard Navier-Stokes (coarse mesh).

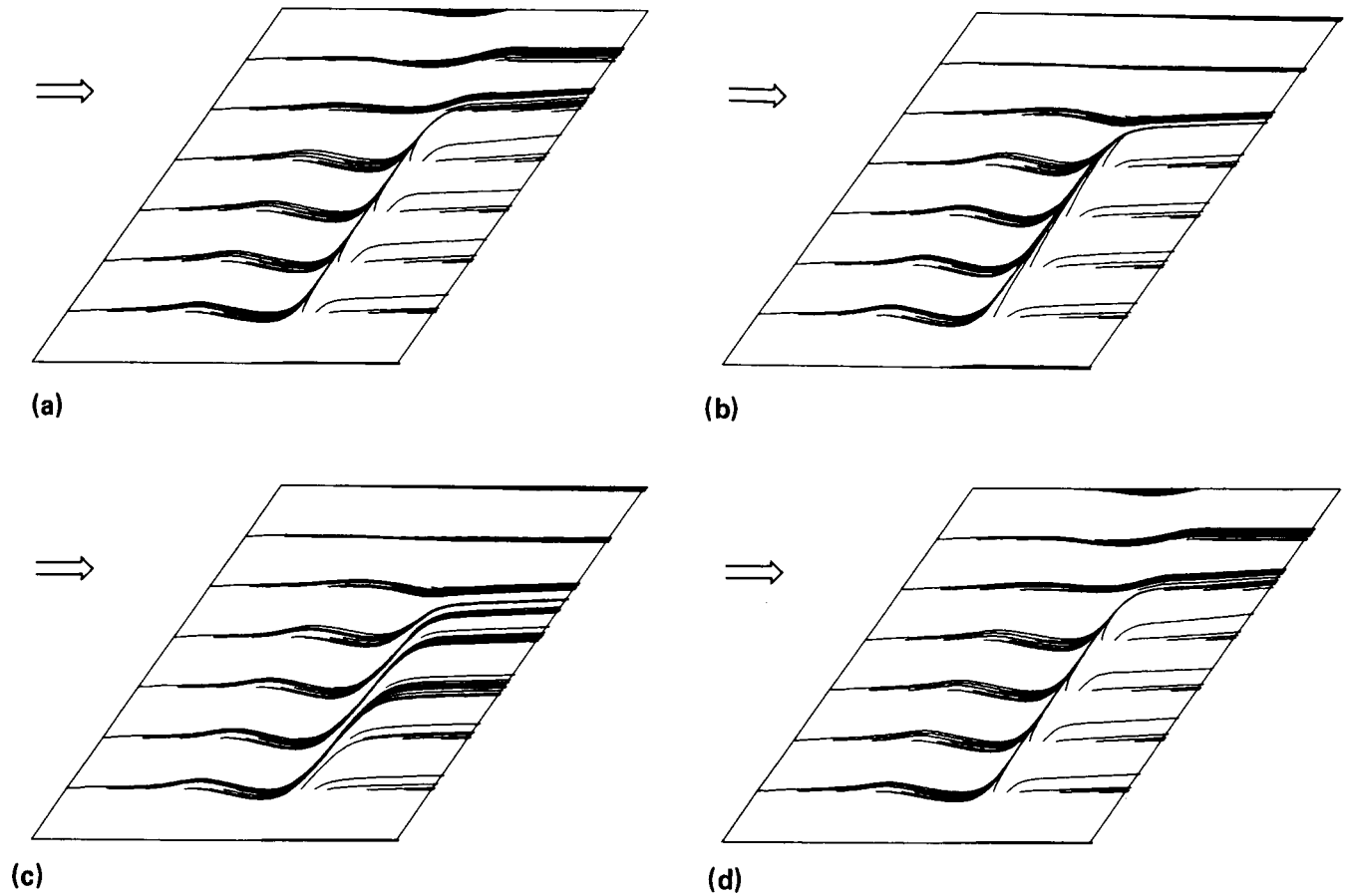


Figure 14. Computed near-surface particle traces for the turbulent flow over a 7.75% sine wave bump with a  $35^\circ$  leading-edge sweep,  $Re = 5 \times 10^5$ ,  $M_\infty = 0.5$ , and  $AR=1$ : a) Fortified Navier-Stokes; b) standard Navier-Stokes (fine mesh); c) standard Navier-Stokes (coarse mesh); d) Fortified Euler.

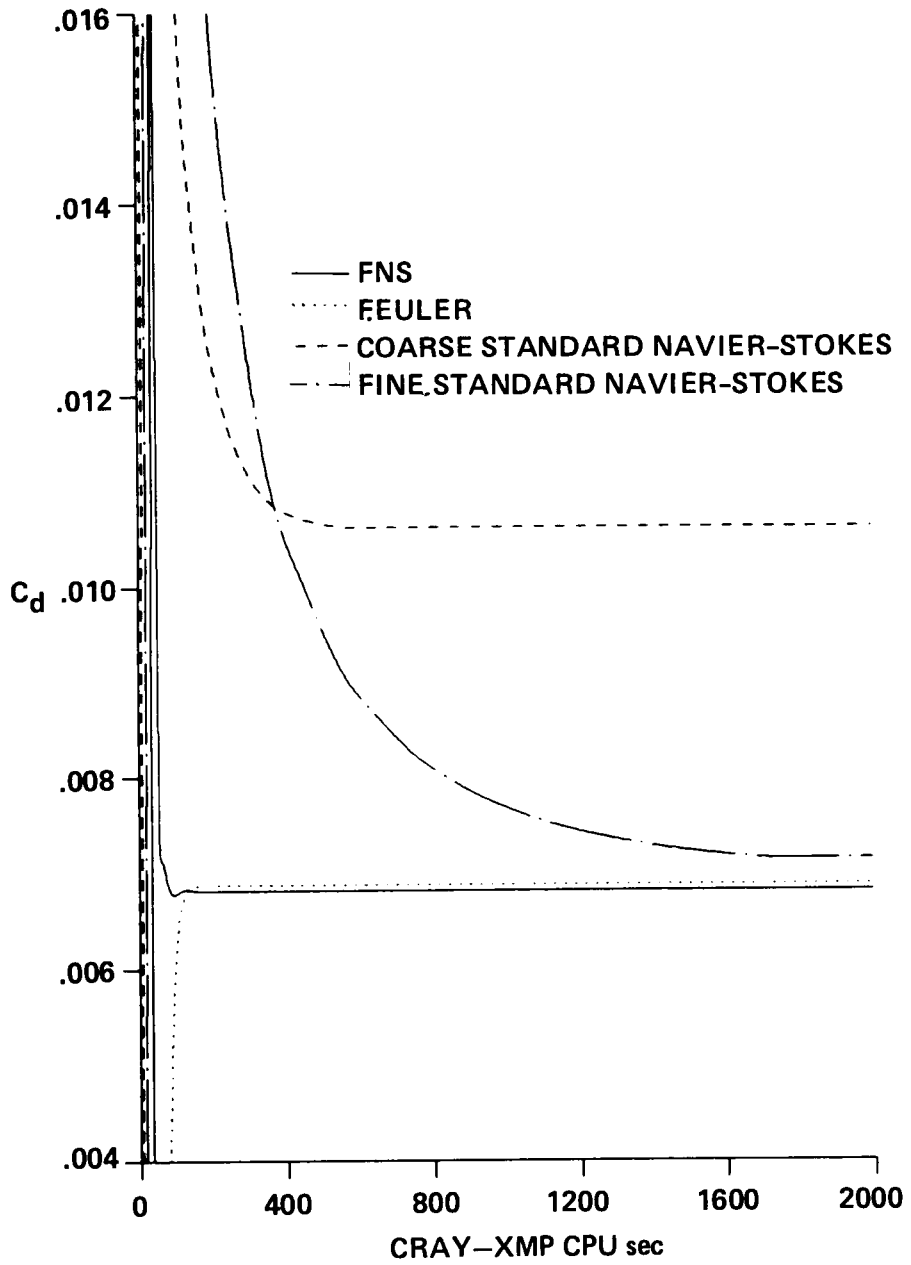


Figure 15. Drag coefficient history versus CRAY-XMP processor time for flow of figure 14.